

Regress Before Construct: Regress Autoencoder for Point Cloud Self-supervised Learning

Yang Liu
College of Computer Science,
Sichuan University
China

Chen Chen
Center for Research in Computer
Vision, University of Central Florida
USA

Can Wang
Laboratory on Multimedia Information
Processing at the Department of
Computer Science, Kiel University
Hangzhou Linxrobot Company
China

Xulin King
Hangzhou GOTHEN Technology Co., Ltd
China

Mengyuan Liu*
Key Laboratory of Machine
Perception, Shenzhen Graduate
School, Peking University
China

ABSTRACT

Masked Autoencoders (MAE) have demonstrated promising performance in self-supervised learning for both 2D and 3D computer vision. Nevertheless, existing MAE-based methods still have certain drawbacks. Firstly, the functional decoupling between the encoder and decoder is incomplete, which limits the encoder's representation learning ability. Secondly, downstream tasks solely utilize the encoder, failing to fully leverage the knowledge acquired through the encoder-decoder architecture in the pre-text task. In this paper, we propose Point Regress AutoEncoder (Point-RAE), a new scheme for regressive autoencoders for point cloud self-supervised learning. The proposed method decouples functions between the decoder and the encoder by introducing a mask regressor, which predicts the masked patch representation from the visible patch representation encoded by the encoder and the decoder reconstructs the target from the predicted masked patch representation. By doing so, we minimize the impact of decoder updates on the representation space of the encoder. Moreover, we introduce an alignment constraint to ensure that the representations for masked patches, predicted from the encoded representations of visible patches, are aligned with the masked patch presentations computed from the encoder. To make full use of the knowledge learned in the pre-training stage, we design a new finetune mode for the proposed Point-RAE. Extensive experiments demonstrate that our approach is efficient during pre-training and generalizes well on various downstream tasks. Specifically, our pre-trained models achieve a high accuracy of **90.28%** on the ScanObjectNN hardest split and **94.1%** accuracy on ModelNet40, surpassing all the other self-supervised learning methods. Our code and pretrained model are public available at: <https://github.com/liuyyy111/Point-RAE>.

CCS CONCEPTS

• Computing methodologies → Shape representations.

KEYWORDS

point clouds, masked point modeling, self-supervised learning, pre-training

1 INTRODUCTION

Self-supervised learning has emerged as a prominent approach for learning representations from unlabeled data, exhibiting exceptional performance across various domains, including natural language processing [3, 22, 41, 42], computer vision [6, 8, 17, 18], and multi-modality learning [20, 40, 60]. By leveraging large-scale unlabeled data for pre-training, models are equipped with robust and versatile representation capabilities, enabling them to offer substantial improvements to downstream tasks through fine-tuning.

Inspired by the great success of BERT [22] in natural language processing (NLP) tasks and MAE [17] in computer vision (CV), masked point modeling (MPM) has been introduced for 3D point cloud pre-training as a new pretext task, which randomly masking some patches of a point cloud and learning to reconstruct the masked patches. As pioneer work, Point-MAE [33], Point-M2AE [59] propose to perform MPM in self-supervised pre-train with transformer [47]. They utilize asymmetric encoder-decoder transformers to apply masked autoencoding for self-supervised learning on 3D point cloud. Specifically, they represent the input point cloud as multiple local patches and randomly mask them with a high ratio to build the pretext task for reconstruction. The encoder aims at capturing high-level latent representations from limited visible patches, and the lightweight decoder is focused to reconstruct masked point patches in coordinate space, then the pre-trained encoder is used to finetune the downstream task.

Despite its effectiveness, the "encoder-decoder" architecture still suffers two main shortcomings. (1) **The functional decoupling between the encoder and decoder is incomplete, which results in a limitation of the encoder's representation learning ability.** The pre-text task aims to reconstruct masked point patches through visible point patches. However, since the encoding representations of the encoder are fed into the decoder as input, the decoder will also optimize the encoding representations during pre-training. Therefore, although the representation quality extracted by the encoder is not good enough, the decoder will

*Corresponding author: liumengyuan@pku.edu.cn

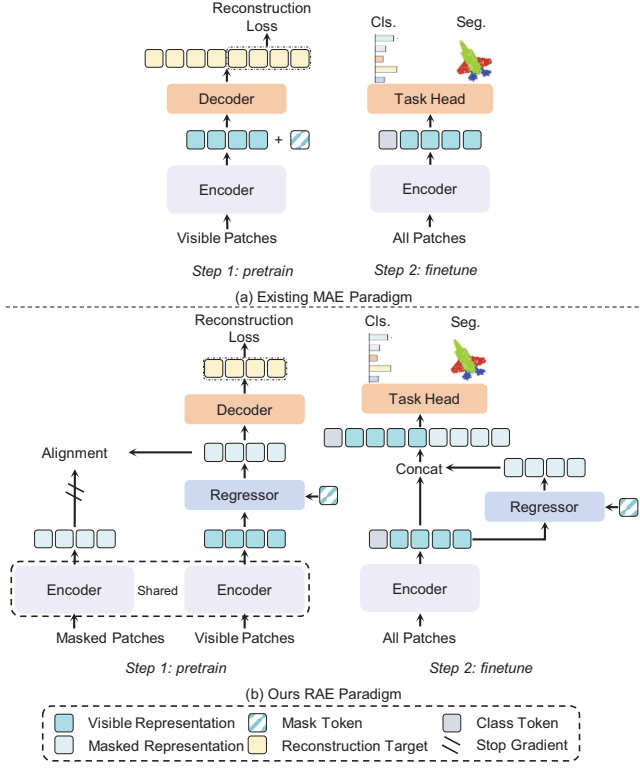


Figure 1: Differences between existing MAE-based methods (a) and our Point-RAE (b). During pre-training, Point-RAE predicts the representation of masked patches and uses it to reconstruct the point cloud. Decoupling the encoder and decoder through the mask regressor enables the decoder to interact with the predicted representation space, avoiding limitations on the encoder’s representation capability. In fine-tuning, both the encoder and mask regressor is optimized to leverage the pre-training knowledge for downstream tasks

also optimize this part. (2) **Downstream tasks solely utilize the encoder and fail to fully leverage the knowledge acquired through the encoder-decoder architecture in the pre-text task.** For instance, masked tokens in the discarded decoder are learnable parameters that can predict masked point patches through visible point patches and further reconstruct them through the decoder. Consequently, the masked token is capable of comprehending the global context of the entire point cloud, but the existing architecture fails to exploit such knowledge efficiently.

As depicted in Figure 1 (b), we propose a new pre-training architecture, Point-RAE, to overcome the limitations mentioned above. The Point-RAE design decouples the encoder and decoder by introducing a mask regressor, which predicts a masked patch representation from the visible patch representation. The predicted masked patch representation is constrained to align with the masked patch representation computed by the encoder. The decoder then reconstructs the predicted masked patch representation. Furthermore, the Point-RAE design expects the encoder to take the responsibility of representation learning through two approaches: first, the

latent representations of visible blocks are not updated in other parts; second, the alignment constraints expect the representations predicted by the mask regressor to also lie in the encoded representation space. By doing so, the decoder does not directly update the representation space of the encoder but directly interacts with the predicted representation space of the mask regressor, **avoiding the limitation on the representation capability of the encoder**. Moreover, the alignment constraint can ensure that the prediction representation space of the mask regressor is consistent with the representation space of the encoder, and it also ensures that the reconstruction function of the decoder is not affected.

We present an additional method to augment the performance of our pre-trained model. In the fine-tuning stage, We encode all patches in the encoder and design different architectures for different tasks to exploit the predictive power of mask regressors. **This methodology maximizes the utilization of pre-trained knowledge and fully exploits the unique features of sparse point clouds.** Consequently, our approach attains state-of-the-art performance on 3D downstream tasks. For instance, Point-RAE achieves a classification accuracy of **90.28%** on the ScanObjectNN [46] hardest split and a classification accuracy of **94.1%** on ModelNet40.

Our contributions are summarized as follows:

- We introduce a novel architecture, Point-RAE, for self-supervised learning on point clouds. Point-RAE introduces the mask regressor to predict the masked patches before the reconstruction task, thereby reducing the direct interaction between the decoder and the encoder representation space, avoiding the limitation on the representation capability of the encoder.
- We propose a new fine-tuning paradigm for Point-RAE, which extends beyond merely fine-tuning the encoder but uses both the encoder and mask regressor in the pre-trained architecture for downstream tasks. Making full use of the predictive ability of the mask regressor can predict more representations of points that do not exist in the original input point cloud, and make up for the sparsity of point cloud data.
- Extensive experimental results by transferring the learned representations to various benchmarks demonstrate the superiority of our proposed Point-RAE compared to recent state-of-the-art self-supervised 3D learning methods. For example, achieving 90.28% accuracy on the most challenging PB-T50-RS benchmark and 94.1% accuracy on ModelNet40.

2 RELATED WORK

2.1 Transformers in Point Clouds.

Transformers were initially proposed to model long-term dependencies in natural language processing (NLP) tasks [47], and have since achieved remarkable success in this area [22, 41] as well as in other domains such as image and video understanding tasks [11, 21, 40, 45, 49]. More recently, there have been efforts to apply Transformers to 3D point cloud data, with PCT [15] and Point Transformer [64] proposing novel attention mechanisms for point cloud feature aggregation, and 3DETR [32] utilizing Transformer blocks and the parallel decoding strategy from DETR [4] for 3D object detection. However, utilizing the end-to-end standard Transformer architecture alone for 3D shape classification has resulted

in lower performance compared to state-of-the-art methods that use point-based [31] and convolution-based [39] approaches.

2.2 3D Point Cloud Pre-training

Supervised learning for point clouds has achieved significant progress with delicately designed architectures [15, 35, 36, 50] and local operators [25, 31, 55]. However, they are confined to limited data domains [46, 52] that they are trained on, and lack satisfactory generalization ability. In contrast, self-supervised pre-training via unlabelled point clouds [63] has shown promising transferable ability, providing a good network initialization for downstream fine-tuning. Mainstream 3D self-supervised approaches employ encoder-decoder architectures to recover input point clouds from transformed representations, including point rearrangement [44], part occlusion [48], rotation [34], downsampling [24], and codeword encoding [56]. Concurrent works also adopt contrastive pre-text tasks between 3D data pairs, such as local-global relations [1, 13, 43], temporal frames [19], and augmented viewpoints [53]. More recent works leverage pre-trained CLIP [40] for zero-shot 3D recognition [55, 60, 65], or introduce masked point modeling [33, 58, 59] as strong 3D self-supervised learners.

2.3 Masked Autoencoders

Recently, masked autoencoders have become one of the hottest research directions and have shown excellent performance in both NLP [22, 28] and CV [2, 7, 54]. Motivated by BERT [22] for masked language modeling and BEiT [2] for masked image modeling, Point-BERT [58] uses the Transformer structure to solve the masked point modeling task, in which the aim of the pre-train task is to predict the discrete tokens. But they do not have explicitly an encoder or a decoder, limiting the representation learning quality. Point-MAE [33] prepend an additional lightweight Transformer structure as a decoder, the encoder only receives visible patches, while the decoder decodes the encoded representations and mask tokens to predict the masked point cloud. Point-M2AE [59] modifies the standard Transformer structure into a pyramid structure and designs a multi-scale masking strategy to incrementally model the spatial geometry and capture the fine-grained and high-level semantics of 3D shapes. In addition, some recent approaches [10, 37, 61] have introduced cross-modalities such as images and text to enhance the pre-training of Masked Point Modeling tasks. There are also some methods [26, 62] that improve the objective of the improved Masked Point Modeling task.

3 PRELIMINARIES: MASKED AUTOENCODER IN POINT CLOUD

We begin by providing a brief overview of the masked autoencoder framework for point clouds. Several previous works, such as [10, 33, 58, 59], have employed this approach to perform 3D point cloud masked autoencoding. This framework typically includes a token embedding module, an asymmetric encoder-decoder transformer, and a reconstruction head that is responsible for reconstructing either masked 3D coordinates [33, 59] or discrete tokens [10, 58].

3.1 Patch Embedding

Due to the quadratic complexity of the self-attention operators, direct input of point clouds into the Transformer Encoder can result in prohibitively high computational costs. To mitigate this issue, existing MAE-based methods [33, 58] adopt a patch embedding strategy that converts input point clouds into 3D point patches.

Specifically, given a raw point cloud $\mathcal{P} \in \mathbb{R}^{N \times 3}$, MAE-based methods initially utilize Furthest Point Sampling (FPS) to sample S points $p_i = 1^S$ as patch centers. Next, k-Nearest Neighbor (k-NN) is employed to gather the k nearest neighbors for each patch center, resulting in a set of 3D point patches $g_i = 1^S$. These 3D point patches are then aggregated into patch embeddings $f_i \in \mathbb{R}^d$ using a mini-PointNet [35], where d denotes the feature dimension. In this way, we obtain a set of patch embeddings $\mathcal{F} \in \mathbb{R}^{S \times d}$ and their center coordinates $\{p_i\}_{i=1}^S$. Each point patch embedding represents a local spatial region and interacts with long-range features with others in the subsequent transformer.

3.2 Asymmetric Encoder-Decoder

To build the pre-text learning targets, Existing MAE-based methods [10, 33, 61] mask the point tokens with a high ratio, e.g., 80%, only using the visible ones $\mathcal{F}_v \in \mathbb{R}^{S_v \times d}$ as input to the transformer encoder, where S_v represents the number of visible patches. Each encoder block comprises a self-attention layer and is pre-trained to comprehend the global 3D shape based on the remaining visible parts. Following encoding, the visible representation \mathcal{F}_v^e is concatenated with a collection of shared learnable masked tokens $\mathcal{T}_m \in \mathbb{R}^{S_m \times d}$ as the input of the decoder, where S_m denotes the number of masked tokens and $S = S_m + S_v$. In the lightweight transformer decoder, the masked tokens learn to capture informative spatial cues from the visible ones, decode the masked tokens \mathcal{T}_m , and output the decoded masked tokens \mathcal{T}_m^e .

3.3 Reconstruction

To reconstruct the masked point patches or tokens, the final layer of the MAE architecture is the prediction head. This head is responsible for generating the output by mapping the learned features to the desired reconstruction target. In existing MAE-based methods [10, 33], a simple fully connected (FC) layer is used as the prediction head. Specifically, taking the output \mathcal{T}_m^e from the decoder, the prediction head projects it to a vector \mathcal{F}_{pre} , which has the same number of dimensions as the reconstruction target. This process allows the model to reconstruct the masked regions based on the learned features and generate the final output.

The reconstruction target for existing MAE-based methods is to recover the coordinates [33] or the discrete token [10] of the points in every masked point patch. To calculate the reconstruction loss, the l_2 Chamfer Distance [12] is used for reconstructing the coordinates, where the prediction point patches \mathcal{F}_{pre} and ground truth \mathcal{F}_{gt} are compared. Alternatively, the negative cosine similarity [10] or cross-entropy loss [58] is used as the reconstruction loss for reconstructing the discrete tokens, where the prediction tokens are compared with the ground truth tokens.

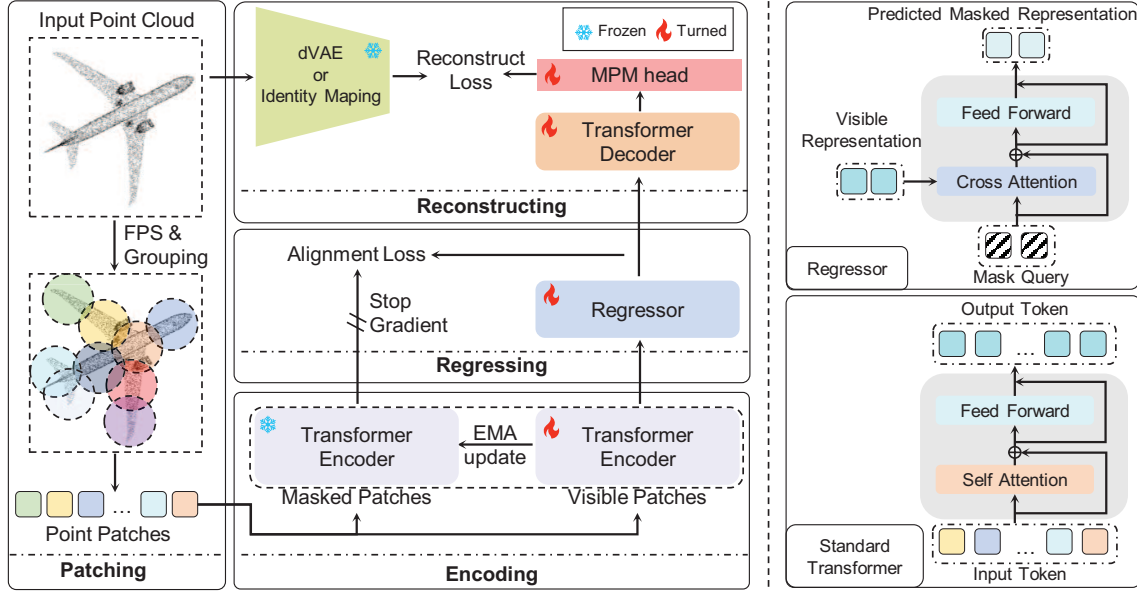


Figure 2: The pre-train pipeline of our proposed Point-RAE. (Left) The training process of pre-training stage consisted of patching, encoding, regressing, and reconstructing. Patching: transfer the point cloud into point patches. Encoding: encode the visible point patches to get visible representation. Regressing: predict the representation of masked point patches. Reconstructing: reconstruct the target by decoding the predicted representation of masked point patches. (Right) The difference between regressor and standard Transformer.

4 POINT REGRESS AUTOENCODER

To address the issue of incomplete functional decoupling between the encoder and the decoder, we propose a novel architecture called the Point-Regression Autoencoder (Point-RAE), as depicted in Figure 2. The key idea of the Point-RAE is to predict masked patches in the encoded representation space from visible patches and then map the predicted representations of masked patches to the corresponding targets, which helps to decouple the encoder and decoder.

4.1 Mask Regressor

The mask regressor is a crucial component of Point-RAE, responsible for predicting the masked representations \mathcal{F}_m^e for the masked patches based on the visible representations \mathcal{F}_v^e output from the encoder. As depicted in Figure 2, the mask regressor consists of a series of *cross-attention* layers and feed-forward networks. To ensure that the mask regressor can learn a robust mapping between visible and masked patches, we introduce the mask query by shifting the mask token of the decoder into the mask regressor. The mask query is a learnable parameter and is shared among all the masked patches. In the mask regressor, we mask tokens as queries, and the output of the previous cross-attention layer consists of keys and values¹ to compute cross-attention and predict representations for mask patches \mathcal{F}_m^e .

¹The key and the value in the first layer is the visible representation \mathcal{F}_v^e .

4.2 Alignment Constraint

The latent representation alignment constraint is imposed on the latent representations \mathcal{F}_m^e of the masked patches predicted by the mask regressor. We feed the masked patches embedding \mathcal{F} into the encoder to generate the representations \mathcal{F}_m^e , the encoder is the same as the one for encoding visible patches, but using an exponential moving average (EMA) to update the weights. We then align the two latent representations \mathcal{F}_m^e and \mathcal{F}_m^e for the masked patches. By doing so, the predicted representations also lie in the encoded representation space and making predictions in the encoded representation space encourages that the encoded representations take on a larger extent of semantics.

4.3 Encoder-Decoder With Mask Regressor

The proposed Point-RAE architecture comprises an encoder, a mask regressor with an alignment constraint, and a decoder. The encoder is similar to previous works and is composed of a sequence of transformer blocks based on *self-attention*. By inputting a set point patch embedding \mathcal{F} , we can obtain the visible representation \mathcal{F}_v^e from the encoder. Subsequently, the visible representation \mathcal{F}_v^e is fed into the mask regressor to predict the masked representation \mathcal{F}_m^e . The predicted masked representation \mathcal{F}_m^e is constrained by alignment with the mask representations \mathcal{F}_m^e computed from the encoder. A lightweight decoder is employed to decode the predicted masked representation \mathcal{F}_m^e to obtain the decoded mask tokens \mathcal{T}_m^e . Noted that the decoder in our Point-RAE architecture differs from previous works in that it is without the mask tokens and the input of the decoder is not the concatenation of the visible

Table 1: Real-world 3D Classification on ScanObjectNN [46]. We report the accuracy (%) on the official three splits of ScanObjectNN. The best performances are in blue.

Method	Year	OBJ-BG	OBJ-ONLY	PB-T50-RS
Supervised Learning Only				
PointNet [35]	2016	73.3	79.2	68.0
PointNet++ [36]	2017	82.3	84.3	77.9
DGCNN [50]	2019	82.8	86.2	78.1
PointCNN [25]	2018	86.1	85.5	78.5
SimpleView [14]	2021	-	-	80.5±0.3
GBNet [39]	2021	-	-	81.0
PRA-Net [9]	2021	-	-	81.0
MVTN [16]	2021	92.6	92.3	82.8
PointMLP [31]	2022	-	-	85.4±0.3
PointNeXt [38]	2022	-	-	87.7±0.4
P2P-RN101 [51]	2022	-	-	87.4
P2P-HorNet [51]	2022	-	-	89.3
with Self-Supervised Representation Learning (FULL)				
Transformer [47]	2017	79.86	80.55	77.24
Point-BERT [58]	2022	87.43	88.12	83.07
MaskPoint [26]	2022	89.30	88.10	84.30
Point-MAE [33]	2022	90.02	88.29	85.18
Point-M2AE [62]	2022	91.22	88.81	86.43
ACT [10]	2023	93.29	91.91	88.21
I2P-MAE [61]	2023	94.15	91.57	90.11
Ours:Point-RAE		95.53	93.63	90.28
with Self-Supervised Representation Learning (LINEAR)				
Point-MAE [33]	2022	82.58±0.58	83.52±0.41	73.08±0.30
ACT [10]	2023	85.20±0.83	85.84±0.15	76.31±0.26
Ours:Point-RAE		86.15±0.33	86.31±0.23	78.25±0.30
with Self-Supervised Representation Learning (MLP-3)				
Point-MAE [33]	2022	84.29±0.55	85.24±0.67	77.34±0.12
ACT [10]	2023	87.14±0.22	88.90±0.40	81.52±0.19
Ours:Point-RAE		88.31±0.20	89.53±0.58	83.01±0.15

representation \mathcal{F}_v^e and mask tokens \mathcal{T}_m , but instead the predicted mask representation \mathcal{F}_m^e . Finally, the decoded mask tokens \mathcal{T}_m^e are fed into the reconstruction head to obtain the reconstruction target \mathcal{F}_{pre} .

The key idea of our Point-RAE architecture is to decouple the encoder and decoder by employing a mask regressor to predict the representation of the masked patches. Unlike the standard Transformer used in the encoder and decoder, the mask regressor comprises a series of cross-attention layers. By utilizing cross-attention, the predicted mask representation can be made independent of the mask query and exist in the same representation space as the encoder output. This approach helps reduce the impact of decoder updates on the representation space of the encoder, thereby ensuring that the encoder’s learned features remain stable.

4.4 Optimization Target

Reconstruction Target. In line with [10], we adopt the dVAE tokens as the reconstruction target. Specifically, given the prediction

Table 2: Synthetic 3D Classification on ModelNet40 [52]. We report the accuracy (%) before and after the voting [27]. The best performances are in blue.

Method	Year	w/o voting	w/ voting
Supervised Learning Only			
PointNet [35]	2016	89.2	90.8
PointNet++ [36]	2017	90.7	91.9
DGCNN [50]	2019	92.9	-
PointCNN [25]	2018	92.2	-
SimpleView [14]	2021	93.9	-
GBNet [39]	2021	93.8	-
PRA-Net [9]	2021	93.7	-
MVTN [16]	2021	93.8	-
PointMLP [31]	2022	94.5	-
PointNeXt [38]	2022	94.0	-
P2P-RN101 [51]	2022	93.1	-
P2P-HorNet [51]	2022	94.0	-
with Self-Supervised Representation Learning (FULL)			
Transformer [47]	2017	91.4	91.8
Point-BERT [58]	2022	93.2	93.8
MaskPoint [26]	2022	93.8	-
Point-MAE [33]	2022	93.8	94.0
Point-M2AE [62]	2022	94.0	-
ACT [10]	2023	93.7	94.0
I2P-MAE [61]	2023	93.7	94.1
Ours:Point-RAE		94.0	94.1

point patches \mathcal{F}_{pre} and ground truth \mathcal{F}_{gt} , we minimize the negative cosine similarity $\mathcal{L}_{cos}(s, t) = 1 - \frac{s \cdot t}{|s||t|}$ to define the reconstruction loss as follows:

$$\mathcal{L}_{rec} = - \sum_{i=1}^S \mathcal{L}_{cos}(\mathcal{F}_{pre}, \mathcal{F}_{gt}) \quad (1)$$

Alignment Target. To align the predicted mask representation \mathcal{F}_m^e with the mask representation \mathcal{F}_m^e , lot of loss functions can be used as alignment target. To keep the feature space consistent, we also minimize the negative cosine similarity as the alignment loss:

$$\mathcal{L}_{align} = - \sum_{i=1}^S \mathcal{L}_{cos}(\mathcal{F}_m^e, sg[\mathcal{F}_m^e]) \quad (2)$$

where $sg[\cdot]$ stands for stop gradient. We study the effect of different loss functions as alignment targets, more details are in Appendix.

The overall pre-training loss function is defined as the sum of the reconstruction and alignment losses:

$$\mathcal{L} = \mathcal{L}_{rec} + \mathcal{L}_{align} \quad (3)$$

4.5 Fine-tune With Regressor

In the fine-tuning stage, existing MAE-based methods direct drop the decoder and only fine-tune the encoder for downstream tasks, which does not take full advantage of the information learned by pre-training, e.g., the mask token in the decoder which has the ability to percept the global structure of the point cloud. We propose a

Table 3: Few-shot classification results on ModelNet40. Overall accuracy (%) without voting is reported. The best performances are in blue.

Method	5-way		10-way	
	10-shot	20-shot	10-shot	20-shot
DGCNN [50]	31.6 ± 2.8	40.8 ± 4.6	19.9 ± 2.1	16.9 ± 1.5
DGCNN+OcCo[48]	90.6 ± 2.8	92.5 ± 1.9	82.9 ± 1.3	86.5 ± 2.2
Transformer [47]	87.8 ± 5.2	93.3 ± 4.3	84.6 ± 5.5	89.4 ± 6.3
Point-BERT [58]	94.6 ± 3.1	96.3 ± 2.7	91.0 ± 5.4	92.7 ± 5.1
MaskPoint [26]	95.0 ± 3.7	97.2 ± 1.7	91.4 ± 4.0	93.4 ± 3.5
Point-MAE [33]	96.3 ± 2.5	97.8 ± 1.8	92.6 ± 4.1	95.0 ± 3.0
Point-M2AE [62]	96.8 ± 1.8	98.3 ± 1.4	92.3 ± 4.5	95.0 ± 3.0
ACT [10]	96.8 ± 2.3	98.0 ± 1.4	93.3 ± 4.0	95.6 ± 2.8
I2P-MAE [61]	97.0 ± 1.8	98.3 ± 1.3	92.6 ± 5.0	95.5 ± 3.0
Ours:Point-RAE	97.3 ± 1.6	98.7 ± 1.3	93.3 ± 4.0	95.8 ± 3.0

new fine-tune paradigm for our Point-RAE, which fine-tune both encoder and mask regressor for downstream tasks.

Since the mask regressor can predict the masked point cloud representation, we can make full use of this ability in downstream tasks, and we can use the existing point cloud structure to predict new ones that do not exist in the original point cloud \mathcal{P} . The representation of coordinates makes up for the sparseness of point clouds. In Section 5.3, we study the different fine-tuning paradigms for different tasks.

5 EXPERIMENT

5.1 Implementation Details

We employed ShapeNet [5] as our pre-training dataset for the purposes of object classification, part segmentation, and few-shot classification. The dataset comprises more than 50,000 distinct 3D models from 55 commonly occurring object categories. Each 3D model is sampled via farthest point sampling (FPS) to obtain 1024 points for each instance. The pre-training process uses an AdamW optimizer [30] and cosine learning rate decay [29], with an initial learning rate of 0.001 and a weight decay of 0.05. The model is trained for 300 epochs with a batch size of 128. We refer to the Appendix for full implementation details and more results.

5.2 Transfer Learning on Downstream Tasks

Transfer Protocol. The study follows the transfer learning protocols for 3D object recognition tasks proposed in [10, 33], which includes three variants:

- † *FULL*: This protocol fine-tunes the pre-trained models by updating all the parameters of the backbone and classification head.
- † *LINEAR*: In this protocol, the classification head consists of a single-layer linear MLP. During fine-tuning, only the parameters of this classification head are updated.
- † *MLP-3*: In this protocol, the classification head consists of a 3-layer non-linear MLP. During fine-tuning, only the parameters of this classification head are updated.

3D Real-World Object Recognition. ScanObjectNN [46] is a challenging point cloud object dataset that is created from real-world scans, comprising of 2,902 samples from 15 categories, and includes background and occlusions, which adds to its complexity. We conducted experiments on three variants of ScanObjectNN, namely OBJ-BG, OBJ-ONLY, and PB-T50-RS. During training, we used simple Rotation as data augmentation following [10], and did not employ any voting methods during testing. The results are presented in Table 1. Our observations are as follows: (i) Our Point-RAE model achieves a significant improvement of +13.94% accuracy averaged on the three variant ScanObjectNN benchmarks, compared to the Transformer *from scratch* baseline under the FULL tuning protocol. (ii) Our Point-RAE outperforms other self-supervised learning methods and achieves the best generalization across all transferring protocols on ScanObjectNN. Specifically, it achieves an average accuracy improvement of +5.3% over Point-MAE on the three variant ScanObjectNN benchmarks. (iii) Our Point-RAE sets a new state-of-the-art performance on ScanObjectNN, achieving 90.28% accuracy on the most challenging PB-T50-RS benchmark when compared to all other methods.

3D Synthetic Object Recognition We conducted an evaluation of our pre-trained model for object classification on the ModelNet40 dataset [52], which comprises 12,311 clean 3D CAD models belonging to 40 object categories. During training, we employed standard random *Scale&Translate* for data augmentation. Moreover, we used the standard voting method [27] during testing. The experimental results are summarized in Table 2, indicating that our Point-RAE method brought significant improvements of +2.6% compared to the Transformer *from scratch* baseline under FULL transferring baseline. Additionally, our results are comparable or better than other self-supervised learning methods.

Few-shot Object Recognition. We conducted fine-tuning experiments on ModelNet40 [52] for few-shot classification, and the results are presented in Table 3. To train the model, we used the same settings and few-shot dataset splits as in previous work [33, 58]. We followed the standard protocol and performed 10 independent experiments for each setting, reporting the mean accuracy with standard deviation. Our Point-RAE model showed significant improvements compared to the Transformer *from scratch* baseline, with an increase in accuracy of +0.5%, +5.4%, +8.7%, and +6.4% for the four few-shot settings, respectively. Furthermore, our Point-RAE consistently outperformed other self-supervised learning methods in all settings.

5.3 Ablation Study

To verify the effectiveness of each component of our Point-RAE, we conduct ablation experiments on the settings of the pre-training stage and the fine-tuning stage respectively. We conduct an extensive ablation study on the most challenging ScanObjectNN PB-T50-RS benchmark with 2,048 input points. In the pre-training stage, we introduced a mask regressor to decouple the encoder and decoder, avoiding the limitation of the encoder’s representation learning ability. In the fine-tuning stage, as shown in Figure 4, we fully use the knowledge learned in the pre-training stage and design a new fine-tuning paradigm. The ablation experiments are shown in Table 4 and Table 5 respectively.

Table 4: Ablation experiments for pre-train settings on the most challenging ScanObjectNN PB-T50-RS benchmark. We report the accuracy (%) of three variants of transfer learning protocols for 3D object recognition. If not specified, the default is: the decoder has depth 2, the mask regressor has depth 2, the alignment loss is negative cosine similarity, the masking ratio is 80%, the pre-training length is 300 epochs and only fine-tune the encoder. Default settings are marked in gray.

Reg. Depth	FULL	LINEAR	MLP-3	Dec. Depth	FULL	LINEAR	MLP-3	Dec.	Reg.	FULL	LINEAR	MLP-3
2	89.89	78.16	82.79	0	89.05	77.81	82.52	✗	✗	88.89	76.31	81.29
4	90.28	78.55	83.16	1	89.98	78.46	82.78	✓	✗	89.42	77.86	82.53
8	90.06	78.58	83.20	2	90.28	78.55	83.16	✗	✓	89.59	77.65	83.01
12	89.93	78.63	83.18	4	90.03	78.48	83.20	✓	✓	90.28	78.55	83.16

(a) Regressor Depth. A deep regressor can improve LINEAR and MLP-3 evaluation.

(b) Decoder Depth. Performance is not sensitive to the decoder depth.

(c) Regress & Construct. Regress and construct are critical to learning representation.

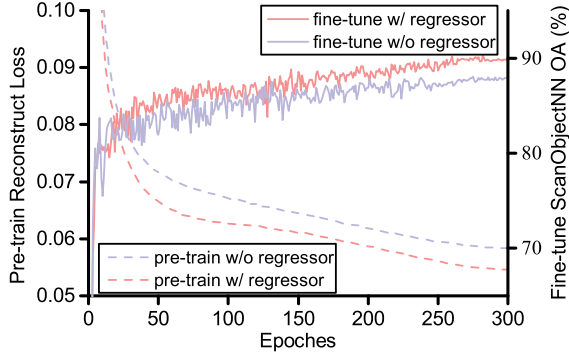


Figure 3: Pre-training reconstruct loss on ShapeNet using models w/ and w/o the mask regressor, and the fine-tuning accuracy (%) on ScanObjectNN PB-T50-RS benchmark with only fine-tuning the encoder.

Regressor Depth. We examine the impact of the mask regressor depth on the pre-training performance of our Point-RAE. Table 4 (a) varies the regressor depth (number of mask regressor blocks). Our analysis reveals that a sufficiently deep regressor is crucial for achieving optimal performance under the *LINEAR* and *MLP-3* evaluation protocols. This finding can be explained by the disparity between transfer learning protocols: a deeper regressor is capable of generating mask representations at a higher level of abstraction, which leads to the learning of more inductive bias during fine-tuning with all parameters. Consequently, a deeper regressor performs best when fine-tuning with limited parameters, such as those in the *LINEAR* and *MLP-3* protocols.

Decoder Depth. In Table 4 (b), we present the results of our experiments on ScanObjectNN using Point-RAE with different decoder depths. We evaluate the model’s performance under three transfer learning protocols. The results show that the performance of the model is not significantly influenced by the decoder’s depth. One possible explanation is that the previous MAE-based method will first implicitly predict the masked patch in the decoder, and then input it into the reconstruction head, while our proposed regressor explicitly predicts the mask patch. We find that the

Table 5: Ablation experiments for effective of fine-tuning paradigm on the most challenging ScanObjectNN PB-T50-RS benchmark. The best performances are in blue.

Model	FULL	LINEAR	MLP-3
(a)	89.58	78.26	82.96
(b)	90.28	78.38	83.10
(c)	89.07	78.55	83.06
(d)	89.89	78.53	83.16

decoder with a 2-layer block achieves the highest accuracy. It is important to note that when the decoder depth is set to 0, we directly use the representation predicted by the mask regressor to achieve the reconstruction task, which is structurally different from previous works [22, 58]. However, we also observe that not including a decoder leads to poor results, which is consistent with previous research.

Regress & Construct. To verify the effectiveness of the two major target regression and construction, we report the ablation results in Table 4 (c). When both the decoder and regressor are removed, the masked modeling architecture is similar to BERT [22], where the encoder sees all tokens, including masked ones, and this leads to poor results. When only the decoder is present and the regressor is removed, our model becomes similar to ACT [10] and shows comparable performance in the three transfer learning protocols. However, due to incomplete functional decoupling between the encoder and decoder, the limitations of the encoder’s representation learning ability still exist. When only the regressor is present and the decoder is removed, the model directly uses the representation predicted by the mask regressor to reconstruct the target, leading to better results than previous methods and demonstrating the effectiveness of the regressor. Finally, when both the regressor and decoder are present, our model achieves the best performance, further demonstrating regress and construct are critical for self-representation learning.

Mask Regressor Benefit to Both Pre-train and Fine-tune. We study the effect of the mask regressor for pre-train and fine-tuning for ScanObjectNN PB-T50-RS benchmark. The results are shown in Figure 3. It can be seen that the reconstruct loss of the model

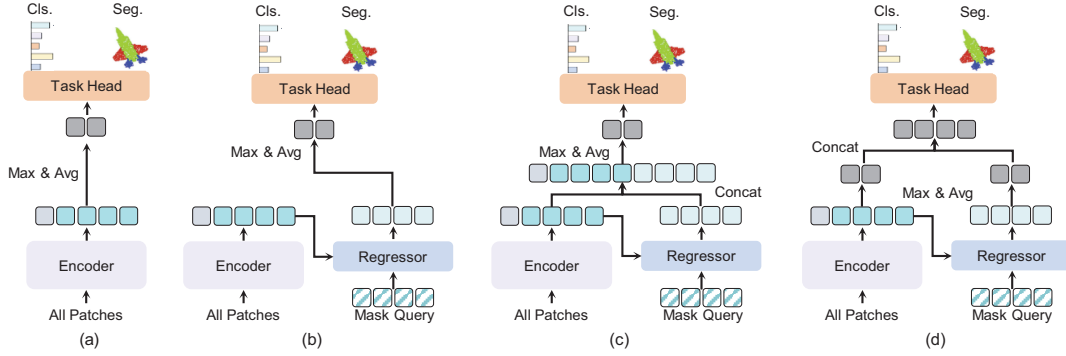


Figure 4: Ablations illustration. (a) the vanilla fine-tuning pipeline, which only uses the encoded representation by Mas&Avg pooling to handle downstream tasks. (b) proposed fine-tuning pipeline, which only uses the predicted representation by Mas&Avg pooling to handle downstream tasks. (c) proposed fine-tuning pipeline, which first concatenates the encoded representation and predicted representation, then feeds into Mas&Avg pooling to handle downstream tasks. (d) proposed fine-tuning pipeline, which first feed encoded representation and predicted representation into Mas&Avg pooling respectively, and concatenates the results to handle downstream tasks.

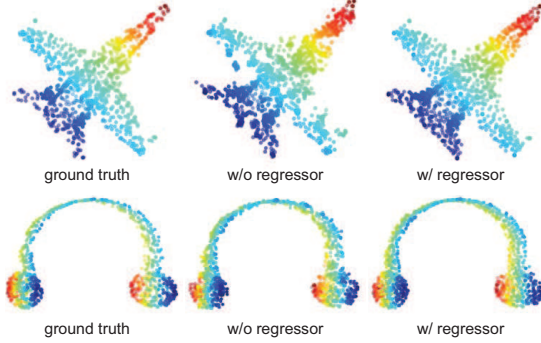


Figure 5: Visualization of reconstruction results of synthetic objects from ShapeNet test set.

w/ mask regressor is consistently lower than the model w/o mask regressor, which converges to a lower value more stably (0.053 vs. 0.060), indicating that the mask regressor brings superior generalization performance of the pretraining construction task. The mask regressor decoupled the encoder and decoder, improving the ability of the encoder to learn generalization representation and alleviate the over-fitting issue during pre-train. The efficacy of the regressor is further demonstrated by the fine-tuning accuracy, where we observe that fine-tuning the model pre-trained with the regressor to the downstream tasks results in improved performance.

Fine-tune with fully using the knowledge of pre-training. We propose a novel fine-tuning paradigm for our Point-RAE and illustrate the different variants in Figure 4. The vanilla fine-tuning pipeline in Figure 4 (a) is commonly employed by existing MAE-based methods to handle downstream tasks. However, our proposed pipeline consists of three different approaches that can be flexibly chosen for different tasks.

As shown in Table 5, all three fine-tune pipeline are outperform the vanilla fine-tuning pipeline. And these pipelines have slightly different effects under different fine-tune settings. The model (b)

achieves the best performance under FULL tuning protocol. A possible explanation is that because the mask regressor can predict the ability of the point cloud representation, the mask regressor can better predict the representation of the key points of the point cloud under FULL tuning protocol, and there is a gap between the pre-training data set and the downstream data set, so The effect is not very good under LINEAR and MLP-3 tuning protocol. The model (c) and (d) achieve better results under LINEAR and MLP-3 tuning protocol than FULL tuning protocol. These models utilize the prediction ability of mask regressor to predict more representation of point clouds which do not exist in the original data. Doing so can improve the shortcomings of point cloud sparsity, and make point cloud features denser by predicting more point representations. Therefore, this paradigm can achieve better results with fine-tuning a small number of parameters.

Construct Visualization. Figure 5 presents a comparison of the reconstruction results obtained by models with and without the mask regressor. The results indicate that the model with the mask regressor can reconstruct high-quality object details. While both models can well reconstruct simple attributes, such as object shapes, the model with the mask regressor can better reconstruct objects with complicated details, such as the airplane wing in the first row, retaining the detailed local geometric information. This result can attest to the mask regressor’s prediction ability for masked patches and improve the point cloud reconstruction effect, which is consistent with the conclusion of Figure 3, and further proves the effectiveness of our proposed Point-RAE method.

6 CONCLUSION

In conclusion, the Point-RAE proposed in this paper is a novel point cloud pre-training method that effectively learns the representation of point clouds for downstream tasks. The Point-RAE employs a masked auto-encoder architecture with a mask regressor to predict the representation of masked patches, which improves the expressive ability of the learned feature space. Additionally, the proposed fine-tuning paradigm further enhances the effectiveness

of the pre-trained model for downstream tasks. Experimental results on various benchmarks demonstrate that Point-RAE outperforms existing methods on different tasks.

7 ACKNOWLEDGEMENT

This work was supported by the National Natural Science Foundation of China (No. 62203476).

REFERENCES

- [1] Mohamed Afham, Isuru Dissanayake, Dinithi Dissanayake, Amaya Dharmasiri, Kanchana Thilakarathna, and Ranga Rodrigo. 2022. Crosspoint: Self-supervised cross-modal contrastive learning for 3d point cloud understanding. In *Proceedings of the IEEE/CVF Conference on Computer Vision and Pattern Recognition*. 9902–9912.
- [2] Hangbo Bao, Li Dong, Songhao Piao, and Furu Wei. 2022. BEiT: BERT Pre-Training of Image Transformers. In *International Conference on Learning Representations*.
- [3] Tom Brown, Benjamin Mann, Nick Ryder, Melanie Subbiah, Jared D Kaplan, Prafulla Dhariwal, Arvind Neelakantan, Pranav Shyam, Girish Sastry, Amanda Askell, et al. 2020. Language models are few-shot learners. *Advances in neural information processing systems* 33 (2020), 1877–1901.
- [4] Nicolas Carion, Francisco Massa, Gabriel Synnaeve, Nicolas Usunier, Alexander Kirillov, and Sergey Zagoruyko. 2020. End-to-end object detection with transformers. In *Computer Vision—ECCV 2020: 16th European Conference, Glasgow, UK, August 23–28, 2020, Proceedings, Part I* 16. Springer, 213–229.
- [5] Angel X Chang, Thomas Funkhouser, Leonidas Guibas, Pat Hanrahan, Qixing Huang, Zimo Li, Silvio Savarese, Manolis Savva, Shuran Song, Hao Su, et al. 2015. Shapenet: An information-rich 3d model repository. *arXiv preprint arXiv:1512.03012* (2015).
- [6] Ting Chen, Simon Kornblith, Mohammad Norouzi, and Geoffrey Hinton. 2020. A simple framework for contrastive learning of visual representations. In *International conference on machine learning*. PMLR, 1597–1607.
- [7] Xiaokang Chen, Mingyu Ding, Xiaodi Wang, Ying Xin, Shentong Mo, Yunhao Wang, Shumin Han, Ping Luo, Gang Zeng, and Jingdong Wang. 2022. Context autoencoder for self-supervised representation learning. *arXiv preprint arXiv:2202.03026* (2022).
- [8] Xinlei Chen and Kaiming He. 2021. Exploring simple siamese representation learning. In *Proceedings of the IEEE/CVF conference on computer vision and pattern recognition*. 15750–15758.
- [9] Silin Cheng, Xiwu Chen, Xinwei He, Zhe Liu, and Xiang Bai. 2021. Pra-net: Point relation-aware network for 3d point cloud analysis. *IEEE Transactions on Image Processing* 30 (2021), 4436–4448.
- [10] Runpei Dong, Zekun Qi, Linfeng Zhang, Junbo Zhang, Jianjian Sun, Zheng Ge, Li Yi, and Kaisheng Ma. 2023. Autoencoders as Cross-Modal Teachers: Can Pre-trained 2D Image Transformers Help 3D Representation Learning?. In *International Conference on Learning Representations*.
- [11] Alexey Dosovitskiy, Lucas Beyer, Alexander Kolesnikov, Dirk Weissenborn, Xiahua Zhai, Thomas Unterthiner, Mostafa Dehghani, Matthias Minderer, Georg Heigold, Sylvain Gelly, et al. 2021. An Image is Worth 16x16 Words: Transformers for Image Recognition at Scale. In *International Conference on Learning Representations*.
- [12] Haoqiang Fan, Hao Su, and Leonidas J Guibas. 2017. A point set generation network for 3d object reconstruction from a single image. In *Proceedings of the IEEE conference on computer vision and pattern recognition*. 605–613.
- [13] Kexue Fu, Peng Gao, Renrui Zhang, Hongsheng Li, Yu Qiao, and Manning Wang. 2022. Distillation with contrast is all you need for self-supervised point cloud representation learning. *arXiv preprint arXiv:2202.04241* (2022).
- [14] Ankit Goyal, Hei Law, Bowei Liu, Alejandro Newell, and Jia Deng. 2021. Revisiting point cloud shape classification with a simple and effective baseline. In *International Conference on Machine Learning*. PMLR, 3809–3820.
- [15] Meng-Hao Guo, Jun-Xiong Cai, Zheng-Ning Liu, Tai-Jiang Mu, Ralph R Martin, and Shi-Min Hu. 2021. Pct: Point cloud transformer. *Computational Visual Media* 7 (2021), 187–199.
- [16] Abdullah Hamdi, Silvio Giancola, and Bernard Ghanem. 2021. Mvtn: Multi-view transformation network for 3d shape recognition. In *Proceedings of the IEEE/CVF International Conference on Computer Vision*. 1–11.
- [17] Kaiming He, Xinlei Chen, Saining Xie, Yanghao Li, Piotr Dollár, and Ross Girshick. 2022. Masked autoencoders are scalable vision learners. In *Proceedings of the IEEE/CVF Conference on Computer Vision and Pattern Recognition*. 16000–16009.
- [18] Kaiming He, Haoqi Fan, Yuxin Wu, Saining Xie, and Ross Girshick. 2020. Momentum contrast for unsupervised visual representation learning. In *Proceedings of the IEEE/CVF conference on computer vision and pattern recognition*. 9729–9738.
- [19] Siyuan Huang, Yichen Xie, Song-Chun Zhu, and Yixin Zhu. 2021. Spatio-temporal self-supervised representation learning for 3d point clouds. In *Proceedings of the IEEE/CVF International Conference on Computer Vision*. 6535–6545.
- [20] Chao Jia, Yinfei Yang, Ye Xia, Yi-Ting Chen, Zarana Parekh, Hieu Pham, Quoc Le, Yun-Hsuan Sung, Zhen Li, and Tom Duerig. 2021. Scaling up visual and vision-language representation learning with noisy text supervision. In *International Conference on Machine Learning*. PMLR, 4904–4916.
- [21] Yifan Jiang, Shiyu Chang, and Zhangyang Wang. 2021. Transgan: Two pure transformers can make one strong gan, and that can scale up. *Advances in Neural Information Processing Systems* 34 (2021), 14745–14758.
- [22] Jacob Devlin Ming-Wei Chang Kenton and Lee Kristina Toutanova. 2019. BERT: Pre-training of Deep Bidirectional Transformers for Language Understanding. In *Proceedings of NAACL-HLT*. 4171–4186.
- [23] Dogyoon Lee, Jaeha Lee, Junhyeop Lee, Hyeonmin Lee, Minhyeok Lee, Sungmin Woo, and Sangyoun Lee. 2021. Regularization strategy for point cloud via rigidly mixed sample. In *Proceedings of the IEEE/CVF Conference on Computer Vision and Pattern Recognition*. 15900–15909.
- [24] Ruihui Li, Xianzhi Li, Chi-Wing Fu, Daniel Cohen-Or, and Pheng-Ann Heng. 2019. Pu-gan: a point cloud upsampling adversarial network. In *Proceedings of the IEEE/CVF international conference on computer vision*. 7203–7212.
- [25] Yangyan Li, Rui Bu, Mingchao Sun, Wei Wu, Xinhan Di, and Baoquan Chen. 2018. Pointcnn: Convolution on x-transformed points. *Advances in neural information processing systems* 31 (2018).
- [26] Haotian Liu, Mu Cai, and Yong Jae Lee. 2022. Masked discrimination for self-supervised learning on point clouds. In *Computer Vision—ECCV 2022: 17th European Conference, Tel Aviv, Israel, October 23–27, 2022, Proceedings, Part II*. Springer, 657–675.
- [27] Yongcheng Liu, Bin Fan, Shiming Xiang, and Chunhong Pan. 2019. Relation-shape convolutional neural network for point cloud analysis. In *Proceedings of the IEEE/CVF conference on computer vision and pattern recognition*. 8895–8904.
- [28] Yinhan Liu, Myle Ott, Naman Goyal, Jingfei Du, Mandar Joshi, Danqi Chen, Omer Levy, Mike Lewis, Luke Zettlemoyer, and Veselin Stoyanov. 2019. Roberta: A robustly optimized bert pretraining approach. *arXiv preprint arXiv:1907.11692* (2019).
- [29] Ilya Loshchilov and Frank Hutter. 2016. Sgdr: Stochastic gradient descent with warm restarts. *arXiv preprint arXiv:1608.03983* (2016).
- [30] Ilya Loshchilov and Frank Hutter. 2017. Decoupled weight decay regularization. *arXiv preprint arXiv:1711.05101* (2017).
- [31] Xu Ma, Can Qin, Haoxuan You, Haoxi Ran, and Yun Fu. 2022. Rethinking Network Design and Local Geometry in Point Cloud: A Simple Residual MLP Framework. In *International Conference on Learning Representations*.
- [32] Ishan Misra, Rohit Girdhar, and Armand Joulin. 2021. An end-to-end transformer model for 3d object detection. In *Proceedings of the IEEE/CVF International Conference on Computer Vision*. 2906–2917.
- [33] Yatian Pang, Wenxiao Wang, Francis EH Tay, Wei Liu, Yonghong Tian, and Li Yuan. 2022. Masked autoencoders for point cloud self-supervised learning. In *Computer Vision—ECCV 2022: 17th European Conference, Tel Aviv, Israel, October 23–27, 2022, Proceedings, Part II*. Springer, 604–621.
- [34] Omid Poursaeed, Tianxing Jiang, Han Qiao, Nayun Xu, and Vladimir G Kim. 2020. Self-supervised learning of point clouds via orientation estimation. In *2020 International Conference on 3D Vision (3DV)*. IEEE, 1018–1028.
- [35] Charles R Qi, Hao Su, Kaichun Mo, and Leonidas J Guibas. 2017. Pointnet: Deep learning on point sets for 3d classification and segmentation. In *Proceedings of the IEEE conference on computer vision and pattern recognition*. 652–660.
- [36] Charles Ruizhongtai Qi, Li Yi, Hao Su, and Leonidas J Guibas. 2017. Pointnet++: Deep hierarchical feature learning on point sets in a metric space. *Advances in neural information processing systems* 30 (2017).
- [37] Zekun Qi, Runpei Dong, Guofan Fan, Zheng Ge, Xiangyu Zhang, Kaisheng Ma, and Li Yi. 2023. Contrast with Reconstruct: Contrastive 3D Representation Learning Guided by Generative Pretraining. *arXiv preprint arXiv:2302.02318* (2023).
- [38] Guocheng Qian, Yuchen Li, Houwen Peng, Jinjie Mai, Hasan Hammoud, Mohamed Elhoseiny, and Bernard Ghanem. 2022. Pointnext: Revisiting pointnet++ with improved training and scaling strategies. *Advances in Neural Information Processing Systems* 35 (2022), 23192–23204.
- [39] Shi Qiu, Saeed Anwar, and Nick Barnes. 2021. Geometric back-projection network for point cloud classification. *IEEE Transactions on Multimedia* 24 (2021), 1943–1955.
- [40] Alec Radford, Jong Wook Kim, Chris Hallacy, Aditya Ramesh, Gabriel Goh, Sandhini Agarwal, Girish Sastry, Amanda Askell, Pamela Mishkin, Jack Clark, et al. 2021. Learning transferable visual models from natural language supervision. In *International conference on machine learning*. PMLR, 8748–8763.
- [41] Alec Radford, Karthik Narasimhan, Tim Salimans, Ilya Sutskever, et al. 2018. Improving language understanding by generative pre-training. (2018).
- [42] Alec Radford, Jeffrey Wu, Rewon Child, David Luan, Dario Amodei, Ilya Sutskever, et al. 2019. Language models are unsupervised multitask learners. *OpenAI blog* 1, 8 (2019), 9.
- [43] Yongming Rao, Jiwen Lu, and Jie Zhou. 2020. Global-local bidirectional reasoning for unsupervised representation learning of 3d point clouds. In *Proceedings*

- of the *IEEE/CVF Conference on Computer Vision and Pattern Recognition*. 5376–5385.
- [44] Jonathan Sauder and Bjarne Sievers. 2019. Self-supervised deep learning on point clouds by reconstructing space. *Advances in Neural Information Processing Systems* 32 (2019).
 - [45] Andreas Steiner, Alexander Kolesnikov, Xiaohua Zhai, Ross Wightman, Jakob Uszkoreit, and Lucas Beyer. 2021. How to train your vit? data, augmentation, and regularization in vision transformers. *arXiv preprint arXiv:2106.10270* (2021).
 - [46] Mikaela Angelina Uy, Quang-Hieu Pham, Binh-Son Hua, Thanh Nguyen, and Sai-Kit Yeung. 2019. Revisiting point cloud classification: A new benchmark dataset and classification model on real-world data. In *Proceedings of the IEEE/CVF international conference on computer vision*. 1588–1597.
 - [47] Ashish Vaswani, Noam Shazeer, Niki Parmar, Jakob Uszkoreit, Llion Jones, Aidan N Gomez, Łukasz Kaiser, and Illia Polosukhin. 2017. Attention is all you need. *Advances in neural information processing systems* 30 (2017).
 - [48] Hanchen Wang, Qi Liu, Xiangyu Yue, Joan Lasenby, and Matt J Kusner. 2021. Unsupervised point cloud pre-training via occlusion completion. In *Proceedings of the IEEE/CVF international conference on computer vision*. 9782–9792.
 - [49] Huiyu Wang, Yukun Zhu, Hartwig Adam, Alan Yuille, and Liang-Chieh Chen. 2021. Max-deeplab: End-to-end panoptic segmentation with mask transformers. In *Proceedings of the IEEE/CVF conference on computer vision and pattern recognition*. 5463–5474.
 - [50] Yue Wang, Yongbin Sun, Ziwei Liu, Sanjay E Sarma, Michael M Bronstein, and Justin M Solomon. 2019. Dynamic graph cnn for learning on point clouds. *Acm Transactions On Graphics (tog)* 38, 5 (2019), 1–12.
 - [51] Ziyi Wang, Xumin Yu, Yongming Rao, Jie Zhou, and Jiwen Lu. 2022. P2P: Tuning Pre-trained Image Models for Point Cloud Analysis with Point-to-Pixel Prompting. In *Advances in Neural Information Processing Systems*.
 - [52] Zhirong Wu, Shuran Song, Aditya Khosla, Fisher Yu, Linguang Zhang, Xiaoou Tang, and Jianxiong Xiao. 2015. 3d shapenets: A deep representation for volumetric shapes. In *Proceedings of the IEEE conference on computer vision and pattern recognition*. 1912–1920.
 - [53] Saining Xie, Jiatao Gu, Demi Guo, Charles R Qi, Leonidas Guibas, and Or Litany. 2020. Pointcontrast: Unsupervised pre-training for 3d point cloud understanding. In *Computer Vision–ECCV 2020: 16th European Conference, Glasgow, UK, August 23–28, 2020, Proceedings, Part III 16*. Springer, 574–591.
 - [54] Zhenda Xie, Zheng Zhang, Yue Cao, Yutong Lin, Jianmin Bao, Zhuliang Yao, Qi Dai, and Han Hu. 2022. Simmim: A simple framework for masked image modeling. In *Proceedings of the IEEE/CVF Conference on Computer Vision and Pattern Recognition*. 9653–9663.
 - [55] Chenfeng Xu, Shijia Yang, Tomer Galanti, Bichen Wu, Xiangyu Yue, Bohan Zhai, Wei Zhan, Peter Vajda, Kurt Keutzer, and Masayoshi Tomizuka. 2022. Image2Point: 3D Point-Cloud Understanding with 2D Image Pretrained Models. In *Computer Vision–ECCV 2022: 17th European Conference, Tel Aviv, Israel, October 23–27, 2022, Proceedings, Part XXXVII*. Springer, 638–656.
 - [56] Yaoqing Yang, Chen Feng, Yiru Shen, and Dong Tian. 2018. Foldingnet: Point cloud auto-encoder via deep grid deformation. In *Proceedings of the IEEE conference on computer vision and pattern recognition*. 206–215.
 - [57] Li Yi, Vladimir G Kim, Duygu Ceylan, I-Chao Shen, Mengyan Yan, Hao Su, Cewu Lu, Qixing Huang, Alla Sheffer, and Leonidas Guibas. 2016. A scalable active framework for region annotation in 3d shape collections. *ACM Transactions on Graphics (ToG)* 35, 6 (2016), 1–12.
 - [58] Xumin Yu, Lulu Tang, Yongming Rao, Tiejun Huang, Jie Zhou, and Jiwen Lu. 2022. Point-bert: Pre-training 3d point cloud transformers with masked point modeling. In *Proceedings of the IEEE/CVF Conference on Computer Vision and Pattern Recognition*. 19313–19322.
 - [59] Renrui Zhang, Ziyu Guo, Peng Gao, Rongyao Fang, Bin Zhao, Dong Wang, Yu Qiao, and Hongsheng Li. 2022. Point-M2AE: Multi-scale Masked Autoencoders for Hierarchical Point Cloud Pre-training. In *Advances in Neural Information Processing Systems*.
 - [60] Renrui Zhang, Ziyu Guo, Wei Zhang, Kunchang Li, Xupeng Miao, Bin Cui, Yu Qiao, Peng Gao, and Hongsheng Li. 2022. Pointclip: Point cloud understanding by clip. In *Proceedings of the IEEE/CVF Conference on Computer Vision and Pattern Recognition*. 8552–8562.
 - [61] Renrui Zhang, Liuhui Wang, Yu Qiao, Peng Gao, and Hongsheng Li. 2023. Learning 3D Representations from 2D Pre-trained Models via Image-to-Point Masked Autoencoders. In *Proceedings of the IEEE/CVF Conference on Computer Vision and Pattern Recognition*.
 - [62] Yabin Zhang, Jiehong Lin, Chenhang He, Yongwei Chen, Kui Jia, and Lei Zhang. 2022. Masked surfel prediction for self-supervised point cloud learning. *arXiv preprint arXiv:2207.03111* (2022).
 - [63] Zaiwei Zhang, Rohit Girdhar, Armand Joulin, and Ishan Misra. 2021. Self-supervised pretraining of 3d features on any point-cloud. In *Proceedings of the IEEE/CVF International Conference on Computer Vision*. 10252–10263.
 - [64] Hengshuang Zhao, Li Jiang, Jiaya Jia, Philip HS Torr, and Vladlen Koltun. 2021. Point transformer. In *Proceedings of the IEEE/CVF international conference on computer vision*. 16259–16268.
 - [65] Xiangyang Zhu, Renrui Zhang, Bowei He, Ziyao Zeng, Shanghang Zhang, and Peng Gao. 2022. PointCLIP V2: Adapting CLIP for Powerful 3D Open-world Learning. *arXiv preprint arXiv:2211.11682* (2022).

Table 7: Ablation study of masking ratio. *Random mask with a high ratio works best.*

Ratio	FULL	LINEAR	MLP-3
20%	89.34	77.65	82.34
40%	89.21	77.81	82.26
60%	89.78	78.11	82.76
80%	90.28	78.55	83.16

Table 8: Alignment Target. *Negative cosine similarity as the alignment loss performs best.*

Target	FULL	LINEAR	MLP-3
NT-Xent loss	89.01	76.81	82.08
Info NCE loss	89.21	77.28	82.16
Mean Square Error	88.34	76.31	81.52
Negative cosine similarity	90.28	78.55	83.16

Table 6: Part segmentation on ShapeNetPart dataset [57]. We report the mIoU over all classes (Cls.) and the mIoU over all instances (Inst.). The best performances are in blue.

Method	Year	Cls.mIoU (%)	Inst.mIoU (%)
Supervised Learning Only			
PointNet [35]	2016	80.39	83.70
PointNet++ [36]	2017	81.85	85.10
DGCNN [50]	2019	82.33	85.20
PointMLP [31]	2022	84.60	86.10
with Self-Supervised Representation Learning (FULL)			
Transformer [47]	2017	83.42	85.10
Point-BERT [58]	2022	84.11	85.60
Point-MAE [33]	2022	-	86.10
ACT [10]	2023	84.66	86.14
Ours:Point-RAE		84.71	86.28

A ADDITIONAL IMPLEMENTATION DETAILS

In this section, we present the detailed model configuration and training settings for pre-training and fine-tuning on downstream tasks. All experiments are conducted on a single Tesla V100 GPU.

In our Point-RAE, for different resolutions of the input point cloud, we divide them into different numbers of patches with a linear scaling. A typical input with $p = 1024$ points is divided into $n = 64$ point patches. For the KNN algorithm, we set $k = 32$ to keep the number of points in each patch constant. In the backbone, the encoder and the decoder consist of Standard Transformer with self-attention, where the encoder has 12 blocks while the decoder has 2 blocks. And the mask regressor consists of Transformer with cross-attention, where the mask regressor has 4 blocks. Each block has 384 hidden dimensions and 6 heads. For downstream tasks, the decoder is discarded.

A.1 Pre-training

We use ShapeNetCore from ShapeNet [5] as the pretraining dataset. ShapeNet is a clean set of 3D CAD object models with rich annotations, including 51K unique 3D models from 55 common object categories. We split the dataset into a training set and a validation set but only conduct pre-training on the training set. For each instance, we sample 1024 points via FPS as input point cloud. Note that we only apply standard random *Scale&Translate* for data augmentation during pre-training.

A.2 Classification

For classification task, we fine-tune both the encoder and the mask regressor. The representation of the encoder is feed into the mask regressor, then taking the output of regressor, we adopt a max pooling & mean pooling operation and concatenate the resulted feature of two pooling. Then, the concatenated feature is fed to the classification head. For the *FULL* tuning protocol, the classification head consists of a MLP. BatchNorm, RELU activation, and Dropout with a ratio of 0.5 are adopted in each layer of MLP. For the *LINEAR* and *MLP-3* tuning protocols, the classification head are a fully connection layer and a MLP respectively, and we only tune the classification head. We apply standard random *Scale&Translate* as data augmentation for ModelNet40 while adopt random *Rotate* for ScanObjectNN. Moreover, we use RSMix [23] in addition to random *Rotation* as data augmentation for ScanObjectNN.

A.3 Few-shot

For few-shot learning, we conduct the evaluation on the ModelNet40 [52] dataset. We fine-tune both the encoder and the mask regressor. The representation of the encoder is feed into the mask regressor, then we adopt a max pooling & mean pooling for the output of representation of both the encoder and the regressor, and add them as the input of the classification head.

A.4 3D Part Segmentation

Same to classification task, we fine-tune both the encoder and the mask regressor, the representation of the encoder is feed into the mask regressor, then taking the output of regressor, we adopt a max pooling & mean pooling operation and concatenate the resulted feature of two pooling. Then, the concatenated feature is fed to the segmentation head.

B ADDITIONAL EXPERIMENTS

3D Part Segmentation To evaluate the geometric understanding performance within objects, we conduct the part segmentation experiment on ShapeNetPart [57]. The synthetic ShapeNetPart is selected from ShapeNet with 16 object categories and 50 part categories, which contains 14,007 and 2,874 samples for training and validation. For fair comparison, we utilize the same segmentation head as previous works [33]. From Table 6, it can be observed that our Point-RAE improves the from scratch baseline by +1.29% and +1.18% Cls. mIoU and Inst. mIoU, respectively. This demonstrates that the mask regressor also benefits the understanding for fine-grained point-wise 3D patterns.

C ADDITIONAL ABLATION STUDIES

To verify the effectiveness of each component of our Point-RAE, we conduct more ablation studies on the three variant ScanObjectNN benchmarks.

Masking Ratio. In Table 7, we present the results of an ablation study where we compare the effects of different masking ratios used for pre-training our Point-RAE model. Our default mask strategy follows the random masking approach proposed in [10, 33], where we randomly sample patches without replacement from the input point cloud data following a uniform distribution. We set the default masking ratio to a high value of 80% for our experiments.

The results in Table 7 demonstrate that using a higher masking ratio with random masking leads to better performance for all three variants of transfer learning protocols.

Alignment Target. The alignment target is a crucial factor in predicting the representation of masked patches, and it has a significant impact on the downstream task results. In Table 8, we compare the performance of different alignment targets. As our proposed Point-RAE uses cosine similarity to compute the reconstruction loss, we find that the negative cosine similarity achieves the best results. Using negative cosine similarity helps to maintain the consistency between the prediction and reconstruction feature spaces during training, which is beneficial for improving the expressive ability of the feature space.

This figure "acm-jdslogo.png" is available in "png" format from:

<http://arxiv.org/ps/2310.03670v1>

This figure "sample-franklin.png" is available in "png" format from:

<http://arxiv.org/ps/2310.03670v1>